R-matrix calculations for opacities: III. Plasma broadening of autoionizing resonances

A K Pradhan[1,2,3]

[1] Department of Astronomy, [2] Chemical Physics Program, [3] Biophysics Graduate Program, Ohio State University, Columbus, Ohio 43210, USA

E-mail: pradhan.1@osu.edu

Abstract. A general formulation is employed to study and quantitatively ascertain the effect of plasma broadening of *intrinsic* autoionizing (AI) resonances in photoionization cross sections. In particular, R-matrix data for iron ions described in the previous paper in the RMOP series (RMOP-II, hereafter RMOP2) are used to demonstrate underlying physical mechanisms due to electron collisions, ion microfields (Stark), thermal Doppler effects, core excitations, and free-free transitions. Breit-Pauli R-matrix (BPRM) cross section for the large number of bound levels of Fe ions are considered, 454 levels of Fe XVII, 1,184 levels of Fe XVIII and 508 levels of Fe XIX. Following a description of theoretical and computational methods, a sample of results is presented to show significant broadening and shifting of AI resonances due to *Extrinsic* plasma broadening as a function of temperature and density. Redistribution of AI resonance strengths broadly preserves their integrated strengths as well as the naturally *intrinsic* asymmetric shapes of resonance complexes which are broadened, smeared and flattened, eventually dissolving into the bound-free continua.

1. Introduction

Resonances arise in most atomic interactions. They are especially important in processes such as (e + ion) scattering and photoionization. At the same time, plasma perturbations markedly affect atomic spectra susceptible to varying temperature, density, and other factors. Whereas a vast body of literature exists on line broadening in laboratory and astrophysics plasma environments [1, 2, 3, 4, 12, 10], there is relatively little work on systematic theoretical treatment of autoionizing resonances that are more readily susceptible to plasma interactions [6, 38], though results have been obtained for K-shell spectra (viz. [23]) observed astrophysically [24]. Stark broadening and other broadening mechanisms for plasmas have been reviewed from the perspective of individual lines and spectrum [21, 8], and in non-local-thermodynamic-equilibrium [11]. However, opacity calculations require a statistical treatment such as implemented in the Opacity Project (hereafter OP [29, 30, 12, 31]).

Resonances are ubiquitous in cross sections, measured and calculated in a variety of ways with ever-increasing precision and resolution. State-of-the-art experimental devices

such as synchrotron based ion storage rings and narrowband photon sources can now resolve resonances in many atomic systems. Coupled-channel calculations, mainly using the R-Matrix method, have been carried out for nearly all elements and ions up to at least iron under OP [12, 13] and, more extensively, the Iron Project (hereafter IP [14]). A prime feature of these calculations is the presence of resonances all throughout the energy ranges of interest. However, resonances are of different types, and exhibit varying shapes, sizes and heights. Their overall resonance strengths may also be computed in analogy with line oscillator strengths for modeling of radiative processes [15].

But the question remains: how are resonance profiles affected by plasma perturbations? To be more precise, how would the *intrinsic* autoionization shape be modified by *extrinsic* particle interactions in a given environment? The complexity of the problem becomes evident when one considers that autoionization profiles are inherently asymmetric, described by the Fano formula for isolated resonances in terms of an asymmetry parameter and energy [17]. But, any singular expression is insufficient to treat infinite overlapping series of AI resonances which, in fact, range from extremely narrow Rydberg resonances approaching series limits, to huge photoexcitation-of-core resonances that span hundreds of eV in energy and considerably alter the background continuum below core excitation threshold [15, 34]. Previous works and conventional approach to plasma modeling of resonances, and collisional-radiative models, generally follow the 'isolated resonance approximation', which treats autoionizing resonances as discrete bound levels and entail the calculation of the oscillator strength at a single energy, followed by a perturbative plasma broadening treatment based on independently calculated autoionization and radiative rates (viz. the Cowan code [41]). Although a physical explanation is lacking, arbitrarily increasing line broadening factors of all lines by up to a factor up to $\sim$100 in atomic structure calculations is found to recover missing solar opacity quantitatively [20].

Ideally, what is needed is a theoretical method that can be translated into a computational algorithm taking into account the variety of resonance shapes and their positions relative to the excited ion core level. Electron-ion interactions in a plasma lead to dominant forms of broadening: Doppler, Stark and electron impact. The Doppler width is approximated by Gaussian that is more narrowly peaked around the line center, and falls off faster, than the other Lorentzian profiles due to Stark and electron impact. The Stark effect due to ions is particularly important for hydrogenic systems when it is linear due to l -degeneracy; a static approximation is sometimes employed since ions move much slower than electrons [1, 16]. In contrast, the electron impact broadening profile is a Lorentzian with much wider effect on the line wings, and as the electron density and the temperature of the plasma increases, electron collisions become the dominant source of broadening. That would especially be the case for weakly bound electrons in doubly-excited autoionizing states, which would be perturbed more than bound electrons considered in line broadening theories.

In this paper we present a computational methodology that aims to incorporate electron impact broadening in a generally applicable manner suitable for laboratory

and astrophysical plasma sources. Without loss of generality, and based on large-scale coupled channel R-matrix calculations ([5, 34]), we consider the photoionization of a complex atomic system, neon-like to fluorine-like iron, Fe XVII $\longrightarrow$ Fe XVIII , in this study as exemplar of applicability to atomic processes in plasmas.

2. Theoretical formulation

We first sketch out the theoretical outline for channel coupling that gives rise to resonances and then the resonance broadening modeled after line broadening due to electron impact.

2.1. Resonances and channel coupling

Autoionizing resonances manifest themselves via inter-channel coupling in the coupled channel (CC) framework. In the CC approximation the atomic system is represented as the 'target' or the 'core' ion of N-electrons interacting with the $(N+1)^{th}$ electron. The $(N+1)^{th}$ electron may be bound in the electron-ion system, or in the electron-ion continuum depending on its energy to be negative or positive. The total wavefunction, Ψ_E, of the (N+1)-electron system in a symmetry $J\pi$ is an expansion over the eigenfunctions of the target ion, χ_i in specific state $S_iL_i(J_i)\pi_i$, coupled with the $(N+1)^{th}$ electron function, θ_i:

$$\Psi_E(e+ion) = A\sum_i \chi_i(ion)\theta_i + \sum_j c_j\Phi_j, \tag{1}$$

where the $\sum_i$ is over the ground and excited states of the target or the core ion. The $(N+1)^{th}$ electron with energy k_i^2 corresponds to a channel labeled $S_iL_i(J_i)\pi_i k_i^2\ell_i(SL(J)\pi)$. The Φ_js are bound channel functions of the (N+1)-electron system that account for short range correlation not considered in the first term and the orthogonality between the continuum and the bound electron orbitals of the target.

Depending upon the total energy E of the (e + ion) system, and the channel energy $k_i^2 > 0$ or $k_i^2 < 0$, a channel may be open or closed relative to an ion level E_i. Inter-channel interactions between open and closed channel wavefunctions result in resonances below the excitation threshold at E_i. If $E < 0$ for all channels then the (e + ion) system is in a pure bound state; otherwise we have a free state with an electron in the continuum and some channels open and some closed. Therefore, the CC wavefunction expansion Eq. (1) may be used to obtain either (e + ion) collision strengths or bound-bound and bound-free radiative parameters such as oscillator strengths and photoionization cross sections.

With reference to Fig. 1, we have the position of a given resonance ω_r corresponding to an excitation threshold E_i in terms of its effective quantum number ν_i as

$$\omega_r = \omega_g + E_i - \frac{(z+1)^2}{\nu_i^2}. \tag{2}$$

That yields

$$\nu_i(\omega_r) = \left[\frac{(z+1)^2}{\omega_g + E_i - \omega_r]}\right]^{1/2}. \tag{3}$$

Typically, there are many excited levels E_i included in coupled channel calculations and may number in the hundreds. Infinite series of resonances $E_i\nu_{n\ell}$ arise and converge on to each level E_i. There can be considerable overlap between weakly bound narrow high-ν Rydberg resonances converging on to and immediately below a given threshold, and deeply bound strong and wide resonances with low ν-values belonging to higher levels. A computational algorithm must successively convolve groups of resonances identified with respect to all ion core levels.

Let $\tilde{\sigma}(\omega')$ be the computed cross section and $\sigma(\omega)$ the convolved cross section such that

$$\sigma(\omega) = \int \tilde{\sigma}(\omega')\phi(\omega,\omega')d\omega', \tag{4}$$

where the profile factor is

$$\phi(\omega,\omega') = \frac{\gamma(\omega)/\pi}{(\omega-\omega')^2 + \gamma(\omega)^2}. \tag{5}$$

2.2. Resonance broadening mechanisms

A general theoretical approximation for scattering of a free electron with an electron in doubly-excited quasi-bound states is necessarily computationally intensive since it needs to be incorporated within a coupled channel framework, and superimposed on *ab initio* calculations of cross sections. Primary broadening mechanisms such as electron collisions, Stark broadening due to ion microfields, and Doppler broadening due to thermal motions need to considered *a priori*. We develop a theoretical treatment that accounts for these physical effects independently within a computational viable procedure.

The parameters in the formulation are derived in analogy with line broadening but modified significantly to apply to AI resonances. In the present formulation we associate the energy to the effective quantum number relative to each threshold $\omega' \to \nu_i$ to write the total width as:

$$\begin{aligned}\gamma_i(\omega,\nu,T,N_e) = \gamma_c(i,\nu,\nu_c) + \gamma_s(\nu_i,\nu_s^*) \\ + \gamma_d(A,\omega) + \gamma_f(f-f;\nu_i,\nu_i'),\end{aligned} \tag{6}$$

pertaining to collisional γ_c, Stark γ_s, Doppler γ_d, and free-free transition γ_f widths respectively, with additional parameters as defined below. Without loss of generality we assume a Lorentizan profile factor that describes collisional-ion broadening which dominates in HED plasmas. We assume this approximation to be valid since collisional profile wings extend much wider as x^{-2}, compared to the shorter range $exp(-x^2)$ for

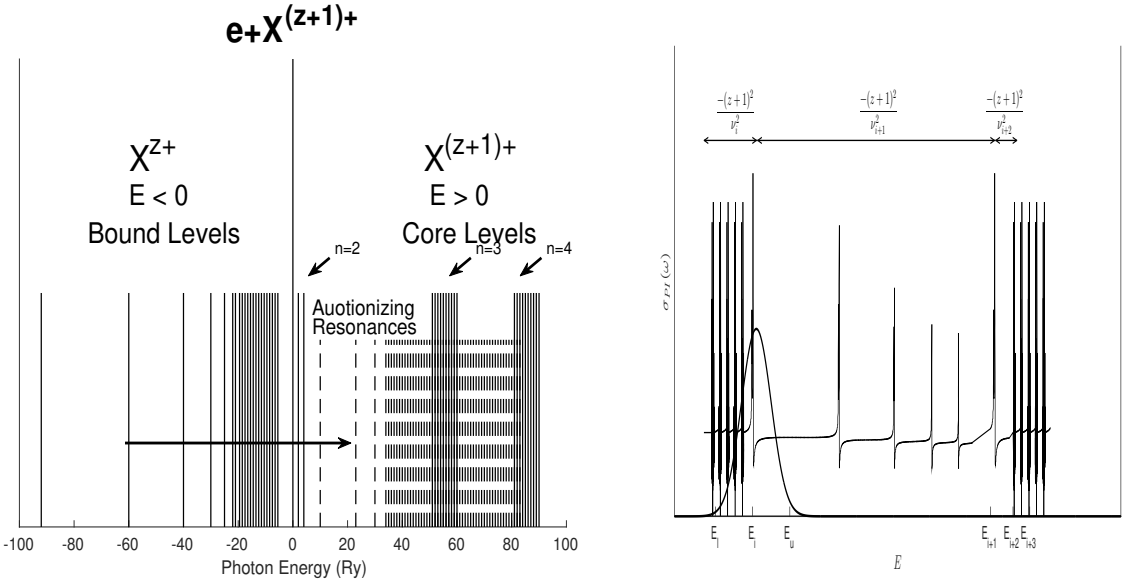

Figure 1. Left: Schematic diagram of a coupled channel calculation for photoionization of bound states (solid lines) of an ion $X^{z+} \rightarrow X^{z+1}$ — AI resonances (dashed lines) correspond to Rydberg series converging on to excited levels of the residual ion with $E = -(z+1)^2/\nu^2$; **Right:** ion thresholds of convergence $E_i,\ E_{i+1},\ E_{i+2},\ E_{i+3}$.... and a Lorentzian profile with lower and upper energy limits (E_ℓ, E_u) spanning narrow high-n resonances below E_i and broader ones above.

thermal Doppler, and $x^{-5/2}$ for Stark broadening (viz. [29]). In principle the limits of integration in Eqs. (4-6) are $\mp\infty$, which are replaced in practical calculations by $\mp\gamma_i/\sqrt{\delta}$, where δ is chosen to ensure full Lorentzian profile energy range and for accurate normalization. Convolution by evaluation of Eqs. (3-6) is carried out for each energy ω throughout the tabulated mesh of energies used to delineate all AI resonance structures, for each cross section, and each core ion threshold.

2.2.1. Electron impact broadening At sufficiently high densities collisional broadening is dominant and mathematically represented by a Lorentizan function (Eq. 5) that correctly approximates the slowly varying behaviour in the line wings. We develop a numerical procedure for convolving cross sections including resonances over a Lorentzian damping width. Given energy dependent cross sections tabulated at sufficiently fine mesh, we first switch the energy variable to the effective quantum number $\nu = z/\sqrt{(E)}$, where $E = \hbar\omega$. In photoionization, we take ω to be the photon frequency; henceforth we shall also employ ω as the energy variable assuming atomic units $\hbar = 1$. The ν is more appropriate since for a resonance it is defined relative to the excited core ion level, as illustrated in Fig. 1.

We consider photoionization of an ion of element X with charge z in an initial state by photon of energy $\hbar\omega$ into the ground or excited level of a residual ion of charge $(z+1)$

$$\hbar\omega + X^{z+} \longrightarrow e + X^{z+1}. \tag{7}$$

It is assumed that unperturbed photoionization cross sections $\tilde{\sigma}_{PI}(\hbar\omega)$ are theoretically computed with sufficient resolution in energy to delineate autoionization profiles. According to the impact approximation [12] we may then represent the damping profile with a Lorentzian expression

$$\phi_\omega(E) = \frac{\gamma/\pi}{[(E+x-E_o)^2 + (\gamma^2]}. \tag{8}$$

In analogy with electron impact damping of bound-bound line transitions, we define E_o as the resonance center, γ as the width and x the energy shift (later we shall assume that $|E - E_o| >> x$). We may further express

$$N_e\gamma = \gamma + ix, \tag{9}$$

where N_e is the electron density and γ is the damping constant which may be written in terms of the electron distribution $f(\epsilon, T)$ at a given temperature T as

$$\gamma(T) = \int_0^\infty vQ_D(\epsilon)f(\epsilon,T)d\epsilon. \tag{10}$$

Given Q_D as the electron impact cross section and a Maxwellian distribution we may obtain the thermally averaged damping rate coefficient

$$\Upsilon_D(T) = \int_0^\infty \Omega_D(\epsilon)exp(-\epsilon/kT)d(\epsilon/kT), \tag{11}$$

where $\Omega(\epsilon)$ is the collision strength. Then

$$\gamma(T) = 2\frac{\hbar^2}{m}\left(\frac{\pi}{mkT}\right)^{1/2}\Upsilon_D \tag{12}$$

.

In Eqs. (8-12) the Υ_D is a complex quantity. However, for small $\delta\omega = (\omega - \omega_o)$ in the one-perturber approximation ([12] and references therein), we have $\gamma = N_e\gamma$ and $\phi_\omega = (\gamma/2\pi)/(\omega - \omega_o)^2$.

Now we establish a correspondence between $\gamma(\omega)$ and the electron impact rate coefficient Υ according to the relation

$$\gamma(\omega) = 2\left(\frac{\pi}{kT}\right)^{1/2} a_o^3 N_e \Upsilon(\nu), \tag{13}$$

where $\Upsilon(\nu)$ is computed at the resonance energy corresponding to $\nu = z/\sqrt{(E)}$, with E in Rydbergs and atomic units $a_o = \hbar = 1$. We now approximate

$$\Upsilon(\nu) \approx G(z) < r_\nu^2 >= G(z)\frac{5\nu^4}{2(z+1)^2}. \tag{14}$$

G(z) is an effective Gaunt factor for electron impact excitation of positive ions, empirically determined for line broadening work in OP [12] to be

$$G(z) = 6.3 - \frac{5.9}{(z+1)}. \tag{15}$$

Table 1. Gaunt factor for electron impact collisional broadening: dependence on temperature T(K), ion charge z and effective quantum number ν of excited levels (Eq. 16) $T = 2 \times 10^6 K,\ z = 16$.

ν	G(T,z,ν)
3.0	1.75
4.0	2.52
5.0	3.12
6.0	3.60
7.0	4.02
8.0	4.37
9.0	4.69
10.0	4.97

The behavior of G(z) with ion charge z and temperature T has been further studied for electron impact broadening, and we adopt an improved expression ([29, 18, 38])

$$G(T, z, \nu_i) = \sqrt{3}/\pi[1/2 + ln(\nu_i kT/z)]. \tag{16}$$

For example, in Table 1 we compare the two expressions and find that they differ significantly for $\nu < 10$, but $G(T, z, \nu \rightarrow G(z)$ as $\nu \rightarrow 10$, and exceeds marginally for $\nu > 10$ when BPRM resonance structure calculations are truncated.

Here ω_g is the ionization energy of the ground state of the photoionizing ion X^{z+}. Then from Eq. (18) we obtain the temperature-density dependent width at each energy

$$\gamma_i(\omega_r; Ne, T) = 5 \left(\frac{\pi}{kT}\right)^{1/2} a_o^3 N_e G(z) \frac{\nu_i^4(\omega_r)}{(z+1)^2}. \tag{17}$$

Evaluating the constants with T(K) and N_e cm$(^{-3})$, we obtain

$$\gamma_i(\omega_r; Ne, T) = 5.2184 \times 10^{-22} \left(\frac{N_e}{T^{1/2}}\right) \left(\frac{G(z)}{(z+1)^2}\right) \nu_i^4(\omega_r). \tag{18}$$

With the transformation of the unbroadened cross section using Eq. (18),

$$\tilde{\sigma}(\omega) \longrightarrow \sigma(\omega; T, N_e), \tag{19}$$

we obtain the temperature-density-energy dependent functional representing the photoionization cross section broadened by electron impact. This greatly expands the scope of the calculations since Eq. (19) implies that the convolution must be carried out at each energy in the tabulated energy mesh (transposed as $E(\omega) \rightarrow \nu$) of unbroadened function $\tilde{\sigma}(\omega)$, with another tabulation for the Lorentzian profile Eq. (8), and for each temperature and electron density. In the next section we describe the procedure developed for such numerical calculations.

Given N core ion levels corresponding to resonance structures,

$$\sigma(\omega) = \sum_i^N \left[\int \tilde{\sigma}(\omega') \left[\frac{\gamma_i(\omega)/\pi}{x^2 + \gamma_i^(\omega)} \right] d\omega' \right]. \tag{20}$$

With $x \equiv \omega' - \omega$, the summation is over all excited thresholds E_i included in the N-level CC or RM wavefunction expansion, and corresponding to total damping width γ_i due to all broadening processes. The profile $\phi(\omega', \omega)$ is centered at each continuum energy ω, convolved over the variable ω' and relative to each excited core ion threshold i .

We employ the following expressions for computations:

$$\gamma_c(i,\nu) \;=\; 5 \left(\frac{\pi}{kT}\right)^{1/2} a_o^3 N_e G(T,z,\nu_i)(\nu_i^4/z^2), \tag{21}$$

where T, N_e , z, and A are the temperature, electron density, ion charge and atomic weight respectively, and ν_i is the effective quantum number relative to each core ion threshold i : $\omega \equiv E = E_i - \nu_i^2/z^2$ is a continuous variable. A factor $(n_x/n_g)^4$ is introduced for γ_c to allow for doubly excited AI levels with excited core levels n_x relative to the ground configuration n_g (e.g. for Fe XVIII $n_x = 3, 4$ relative to the ground configuration $n_g = 2$).

2.2.2. Stark broadening A treatment of the Stark effect for complex systems entails two approaches, one where both electron and ion perturbations are combined (viz. [19, 38]), or separately (viz. [12, 29]) employed herein. Excited Rydberg levels are nearly hydrogenic and ion perturbations are the main broadening effect, though collisional broadening competes significantly increasing with density as well as ν_i^4 (Eq. 14). For bound levels in a plasma microfield of strength F, the Stark sub-levels of a level n span a range given by the highest component (n, k_{max}) with energy (viz. [12, 29])

$$E(n, k_{max}) = -\frac{z^2}{n^2} + \frac{3}{z} n(n-1)F \tag{22}$$

and the lowest component of sub-level $((n+1), k_{min})$ with energy

$$E(n+1, k_{min}) = -\frac{z^2}{(n+1)^2} - \frac{3}{z} n(n+1)F. \tag{23}$$

In deriving occupation probabilities in the Mihalas-Hummer-Däppen equation-of-state (MHD-EOS) [31] used in OP work [12], a critical field strength F_c is calculated when Stark broadening renders these two components equal, and Stark ionization dissolves level n into the continuum. The total Stark width of a given n -complex is $\approx (3F/z)n^2$. Assuming the dominant ion perturbers to be protons and density equal to electrons, N_e =N_p, and replacing n by the effective quantum number ν_i relative to each excited threshold of an ion with charge z, we take $F = [(4/3)\pi a_o^3 N_e)]^{2/3}$, as employed in MHD-EOS for Stark broadening in Eq. (6)

$$\gamma_s(\nu_i, \nu_s^*) = [(4/3)\pi a_o^3 N_e]^{2/3} \nu_i^2. \tag{24}$$

In addition, in employing Eq. (6) a Stark ionization parameter $\nu_s^* = 1.2 \times 10^3 N_e^{-2/15} z^{3/5}$ is introduced such that AI resonances may be considered fully dissolved into the continuum for $\nu_i > \nu_s^*$, analogous to but distinct from the Inglis-Teller series limit [32], or the Stark ionization of *bound* (not AI) energy levels as considered in the MHD-EOS [31].

All calculations are carried out with and without ν_s^* as shown later in Table 2, and illustrated in the Figs. 3, 4, 5 presented herein (red and blue curves respectively). Results are practically indistinguishable with and without Stark ionization cut-off, and effect on redistribution of differential oscillator strength or opacities. However, ν_s^* is a parameter that should prove to be useful in further extension of plasma effects including Debye screening, as discussed later.

2.2.3. Thermal Doppler broadening The Doppler width is:

$$\gamma_d(A, T, \omega) = 4.2858 \times 10^{-7} \sqrt{(T/A)}, \tag{25}$$

where ω is *not* the usual line center but taken to be each AI resonance energy.

2.2.4. Free-free transitions broadening The last term γ_f in Eq. (6) accounts for free-free transitions among autoionizing levels with ν_i, ν_i' such that

$$X_i + e(E_i, \nu_i) \longrightarrow X_i' + e'(E_i', \nu_i'). \tag{26}$$

The large number of free-free transition probabilities for $+ve$ energy AI levels $E_i, E_i' > 0$ may be computed using RM or atomic structure codes (viz. [33, 37]). Free-free transitions are not considered in the results in Figs. 2 and 3 but included in the results discussed in Table 1, although it is found to be practically negligible.

3. Computational algorithm

In order to elicit and illustrate important physical features of the formulation, we sketch a few salient features of the mathematical algorithm developed to implement the procedure (numerical details and the computer program will be presented elsewhere).

We have re-defined the Lorentzian profile Eq. (5) as in Eq. (8), using a damping rate coefficient Eqs. (10-13) and Maxwellian electron distribution, dependent on electron density and temperature as in Eqs. (17-18). Numerical evaluation scheme based on this formulation requires several practical considerations to be incorporated in the computational algorithm and computer program.

3.1. Profile limits

The limits of integration in Eq. (4) are determined by the extent of the Lorentzian factor in Eq. (8). It needs to be ensured that the profile extends into the resonance wings and/or approaches the background continuum without loss of accuracy. Measuring the

energy spread relative to the resonance center $\omega = \omega_r$, we note that according to Eq. (13) $\omega = \omega_g + E_i$, with respect to the ionization potential and the target excitation energy E_i above the ground state of the residual ion. Then the profile maximum is (Eq. 8)

$$\phi_{max}(\omega = \omega_r) = \frac{1}{\pi\gamma(\omega)}. \tag{27}$$

We introduce an accuracy parameter δ and choose the profile limits $\pm\omega_o$ such that

$$\phi(\omega = \omega_o) = \delta\phi_{max} = \frac{\delta}{\pi\gamma(\omega)}. \tag{28}$$

Then,

$$\frac{\delta}{\pi\gamma(\omega)} = \frac{\gamma(\omega)/\pi}{(\omega - \omega_o)^2 + \gamma^2(\omega)}. \tag{29}$$

Or,

$$(\omega - \omega_o)^2 = \gamma^2(\omega)\left(\frac{1}{\delta} - 1\right). \tag{30}$$

For small δ,

$$(\omega - \omega_o)^2 \approx \frac{\gamma^2(\omega)}{\delta}. \tag{31}$$

Therefore, $|\omega - \omega|$ limits the convolution profile such that

$$\omega - \omega_o = \pm\frac{\gamma}{\delta^{1/2}}. \tag{32}$$

Whereas Eq.(4) using Eq. (5) has an analytical solution in terms of $tan^{-1}(x/\gamma)/\gamma$ evaluated at limiting values of $x \to \mp\gamma/\sqrt{\delta}$, its evaluation for practical applications entails piece-wise integration across multiple energy ranges spanning many excited thresholds and different boundary conditions. For example, the total width γ is very large at high densities and the Lorentzian profile may be incomplete above the ionization threshold and therefore not properly normalized. We obtain the necessary redward left-wing correction for partial renormalization as

$$\lim_{a\to-\gamma/2\sqrt{\delta}} \int_a^{+\gamma/\sqrt{\delta}} \phi(\omega, \omega')d\omega' = \left[\frac{1}{4} - \frac{tan^{-1}(\frac{a}{\gamma/2\sqrt{\delta}})}{\pi}\right], \tag{33}$$

where a is the lower energy range up to the ionization threshold, reaching the maximum value $-\gamma/2\sqrt{\delta}$. The parameter δ is generally chosen to be 10^{-2} so that the total profile ranges over 10γ.

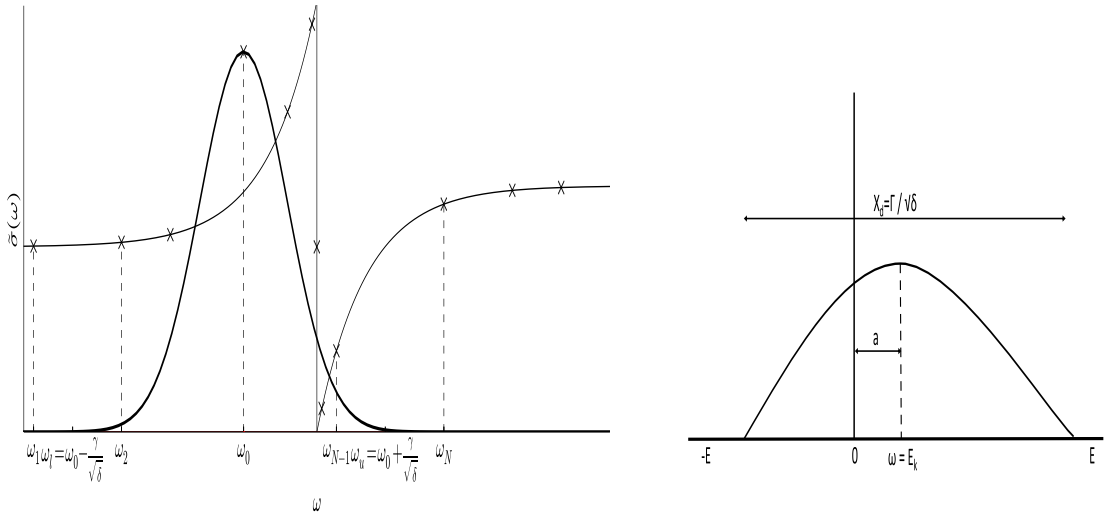

Figure 2. Left: Tabulated cross sections at energies ($hbar = 1$) $\omega_1, ...\omega_N$ spanning a resonance centered at ω_o, and Lorentzian profile with lower and upper limits $\omega_\ell = \omega_o - \gamma/sqrt(\delta), \omega_u = \omega_o + \gamma/sqrt(\delta)$. Point-by-point normalized profile convolution ensures a complete quadrature. **Right:** Incomplete profile centered at $\omega = E_k$ with lower energy redward cut-off at ionization threshold on the left and partial renormalization as in Eq. 31.

3.2. Convolution quadrature

The complexity of the problem arises from the following main factors: (i) wide variety of narrow and broad resonances, (ii) overlapping infinite Rydberg series belonging to a large number of excitation thresholds of the target ion, and (iii) Lorentzian profiles that vary at each energy on a mesh that is independent of the tabulated energy mesh for the original cross section. The schematics are described in Fig. 2.

Numerically, we need to evaluate the integrand in Eq. (20) using Eq. (9), i.e.

$$\sigma(\omega) = \sum_i \left[\int \tilde{\sigma}(\omega') \left[\frac{\gamma_i(\omega)/\pi}{(\omega - \omega')^2 + \gamma_i^(\omega)} \right] d\omega' \right]. \tag{34}$$

Here the summation is over all excitation thresholds E_i included in the CC wavefunction expansion (Eq. 1) and corresponding damping widths γ_i. The profile $\phi(\omega', \omega)$ is centered at ω; we define $x \equiv \omega' - \omega$ (note change of order of variables which is immaterial), then

$$\sigma(\omega) = \sum_i \left[\frac{\gamma_i}{\pi} \int_{-\frac{\gamma_i}{\sqrt{\delta}}}^{+\frac{\gamma_i}{\sqrt{\delta}}} \frac{\tilde{\sigma}(x)}{x^2 + \gamma_i^2} dx. \right] \tag{35}$$

This equation requires discrete summation over all target ion thresholds, and piecewise integration over normalized profile at each energy. First, we consider the endpoints with lower energy limit $x_\ell \equiv -(\omega_o - \omega) = -\gamma_i/\sqrt{\delta}$, and upper limit $x_u \equiv +(\omega_o - \omega) = +\gamma_i/\sqrt{\delta}$. Let the tabulated energy mesh be $\omega_1, \omega_2, ...\omega_N$. Then

$x_1 = \omega_1 - \omega$, $x_2 = \omega_2 - \omega$, ...,$x_N = \omega_N - \omega$. Assuming the lower limit x_ℓ to lie between $x_1 < x_\ell < x_2$; and the upper limit x_u between $x_{N-1} < x_u < x_N$, we have

$$\sigma(\omega) = \sum_i \left[\frac{\gamma_i}{\pi} \int_{x_\ell}^{x_2} \frac{\tilde{\sigma}(x)}{x^2 + \gamma_i^2} dx + \int_{x_3}^{x_4} (...) dx + ... \right] \tag{36}$$

$$+ .... + \left[\int_{x_{N-1}}^{x_N} (.....) dx \right]. \tag{37}$$

3.3. Interpolation and evaluation

Each of the raw originally tabulated unbroadened cross sections $\tilde{\sigma}(\omega')$ needs to be interpolated on to the resonance profile mesh. A linear interpolation is sufficient for precision since the CC calculations are usually carried out at a fine mesh to resolve most autoionizing resonances up to $\nu_i \leq= \nu_{max} = 10$ below each target threshold E_i. Suppose the transposed energy mesh ω on to the resonance profile is represented by linearly interpolated segments $a_j + b_j x$ with a_j, b_j coefficients such that, $x_\ell = -\gamma/\sqrt{(}\delta) < x < x_2 \longrightarrow \sigma_1(\omega) = a_1 + b_1 x$, $b_1 = [\tilde{\sigma}(\omega_2) - \tilde{\sigma}(\omega_1)]/(\omega_2 - \omega_1)$; $x_2 < x < x_3 \longrightarrow \sigma_2(\omega) = a_2 + b_2 x$, $b_2 = [\tilde{\sigma}(\omega_3) - \tilde{\sigma}(\omega_2)]/(\omega_3 - \omega_2)$;..... $x_(N) < x < x_u = +\gamma/\sqrt{(}\delta) \longrightarrow \sigma_N(\omega) = a_N + b_N x$, $b_N = [\tilde{\sigma}(\omega_N) - \tilde{\sigma}(\omega_{N-1}]/(\omega_N - \omega_{N-1})$. Then for all thresholds i,

$$\sigma(\omega) = \sum_i \frac{\gamma_i}{\pi} \left[\sigma_1(\omega) + \sigma_2(\omega) + ... + \sigma_N(\omega) \right]. \tag{38}$$

It is understood that the interpolation and summation is carried out with respect to profiles corresponding to all target ion thresholds at E_i. Having determined coefficients a_j, b_j we need to evaluate expressions for each segment as

$$\sigma_j(\omega) = \frac{\gamma_i}{\pi} \int_{x_j}^{i} x^{j+1} \frac{(a_j + b_j x)}{x^2 + \gamma^2} dx. \tag{39}$$

Evaluating separately,

$$\sigma_j(\omega) = a_j \left[\frac{tan^{-1}(x/\gamma_i)}{\gamma_i} \Big|_{x_j}^{x_{j+1}} \right] + \frac{b_j}{2} \left[ln(x^2 + \gamma_i^2) \Big|_{x_j}^{x_{j+1}} \right]. \tag{40}$$

For clarity we have avoided the use of double scripts (i, j), one with respect to thresholds E_i and the other for interpolation between respective resonance profile segments. But in principle we may represent the final values of the cross sections convolved over all resonances at the transposed energy mesh $\omega' \rightarrow \omega$ as

$$\sigma(\omega) = \sum_{i,j} \sigma_j^i(\omega), \tag{41}$$

subsuming all target ion levels (Fig. 1 and Eq. 1) and interpolation into the computational algorithm. Finally, we compute broadened cross sections at the same energy mesh as the unbroadened cross sections $\tilde{\sigma}(\omega')$ so that there is one-to-one correspondence $\omega' \rightarrow \omega$. However, we note that the *intermediate* energy mesh of the Lorentzian profile is independent, and interpolated in accordance with the damping width Eq. (11-12) at each energy.

3.4. Computer program

A general program for convolving AI resonances has been written and will be reported elsewhere. Here we note a few of the main features. The primary loops in the program are over electron temperature T_e, density N_e, and target thresholds E_i. The input is the unbroadened CC cross sections tabulated at a sufficiently fine mesh to resolve resonances so that convolution, interpolation and integration do not result in loss of accuracy. The accuracy parameter δ is chosen to be in the range $10^{-2} - 10^{-6}$; more importantly, it is ensured that the convolved cross sections have converged, physically implying that the resonance wings have merged into the continuum. The CPU time required depends mainly on the density which determines the total width γ; for example, in the reported calculations for Fe XVII at T=2×10^6K it is few minutes for $N_e = 10^{21}$ cc and ∼3 hours for N_e =10^{24}cc.

The program is suitable as a module within a post-processing program for CC cross sections with AI resonances for photoionization, electron-ion collisions and recombination, intended for practical application in specified temperature-density range.

4. Results and discussion

The complexity and magnitude of RMOP computations has been studied using photoionization data for a large number of bound levels of the three Fe ions described in RMOP2. Since AI plasma broadening must be carried at each temperature-density pair, the resulting cross sections constitute a huge amount of data required for opacities calculations in HED plasma sources. In this section we discuss a small sample of results for those Fe ions to illustrate some physical features.

4.1. Fe XVII *: Temperature-Density dependence*

Owing to its closed shell ground configuration and many excited n-complexes of configurations, Ne-like Fe XVII is of considerable importance in astrophysical and laboratory plasmas, as described in a number of previous works ([35] and references therein). The Fe XVII BPRM calculations are carried out with 218 fine structure levels dominated by $n = 2, 3, 4$ levels of the core ion Fe XVIII . The computed Fe XVII bound levels ($E < 0$) are dominated by configurations $1s^2 2s^2 2p^6(^1S_0), 1s^2 2s^p 2p^q n\ell, [SLJ]$ $(p, q = 0 - 2,\ n \leq 10,\ \ell \leq 9,\ J \leq 12)$. The core Fe XVII levels included in the CC calculation for the (e + Fe XVIII) →Fe XVII system are:$1s^2 2s^2 2p^5(^2P^o_{1/2,3/2}), 1s^2 2s^2 2p^q, n\ell, [S_i L_i J_i]$ $(p = 4, 5,\ n \leq 4, \ell \leq 3)$. The Rydberg series of AI resonances correspond to $(S_i L_i J_i)\ n\ell,\ n \leq 10, \ell \leq 9$, with effective quantum number defined as a continuous variable $\nu_i = z/\sqrt{(E_i - E)}$ $(E > 0)$, throughout the energy range up to the highest 218^{th} Fe XVIII core level; the $n = 2, 3, 4$ core levels range from E=0-90.7 Ry ([34, 35]). The Fe XVII BPRM calculations were carried out resolving the bound-free cross sections at ∼40,000 energies for 454 bound levels with AI resonance structures (in total 587 bound levels are considered, but the higher lying

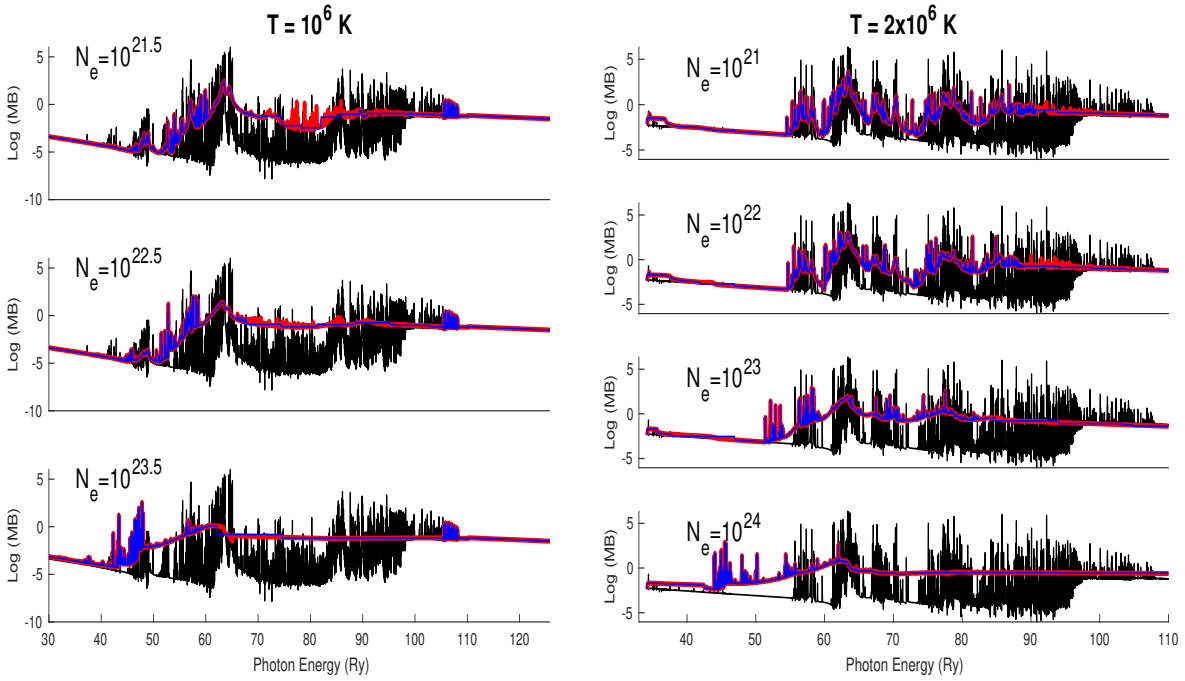

Figure 3. Plasma broadened photoionization cross sections for $\hbar\omega$ + Fe xvii $\rightarrow$ e + Fe xviii of the bound level $2s^2 2p^5[^2P^o_{3/2}]4d(^1F^o_3)$ (left, ionization energy 17.626 Ry), level $2s^2 2p^5[^2P^o_{3/2}]3p(^3D_2)$ (right, ionization energy 37.707 Ry) along two isotherms $T = 1 \times 10^6$K (left) and $T = 2 \times 10^6$K (right), and electron densities as shown in each panel: black — unbroadened, red — broadened, blue — broadened with Stark ionization cut-off ν^*_s (Table 1). Rydberg series of AI resonance complexes with $\nu_i \leq 10$ belonging to 217 excited Fe xviii levels E_i broaden and shift with increasing density, also resulting in continuum raising and threshold lowering.

levels are included to ensure convergence and completeness as discussed in paper P4, and do not significantly contribute to opacities calculations). Given 217 excited core levels of Fe xviii , convolution is carried out at each energy or approximately 10^9 times for each (T,N_e) pair.

Fig. 3 (left) displays detailed results for plasma broadened and unbroadened photoionization cross section of one particular excited level $2s^2 2p^5[^2P^o_{3/2}]3p(^3D_2)$ (left, ionization energy 37.707 Ry) of Fe xvii along isotherm $T = 10^6$K at three representative densities (note the $\sim$10 orders of magnitude variation in resonance heights along the Y-axis). The main feature evident in the figure are as follows. (i) AI resonances begin to show significant broadening and smearing of a multitude of overlapping Rydberg series at $N_e = 10^{21}$cc. The narrower high-n l resonances dissolve into the continua but stronger low-n l resonance retain their asymmetric shapes with attenuated heights and widths. (ii) As the density increases by one to two order of magnitude, to $N_e = 10^{22-23}$cc, resonance structures not only broaden but their strengths shift and redistributed over a wide range determined by total width $\gamma(\omega, \nu_i, T, N_e)$ at each energy $\hbar\omega$ (Eq. 6). (iii) Stark ionization cut-off (Table 1) results in step-wise structures that represent

the average due to complete dissolution into continua. (iv) The total AI resonance strengths are conserved, and integrated values generally do not deviate by more than 1-2%. For example, the three cases in Fig. 3 (left): unbroadened structure (black), and broadened without (red) and with Stark cut-off (blue), the integrated numerical values are 59.11, 59.96, 59.94 respectively. This is also an important accuracy check on numerical integration and the computational algorithm, as well as the choice of the parameter δ that determines the energy range of the Lorentizan profile at each T and N_e; in the present calculations it varies from δ = 0.01-0.05 for N_e =10^{21-24}cc.

Fig. 3 (right) shows similar results to Fig. 3 (left) for another excited Fe XVII level $2s^2 2p^5[^2P^o_{3/2}]4d(^1F^o_3)$ (ionization energy 17.626 Ry), along a higher temperature 2×10^6K isotherm at different intermediate densities. Both Figs. 2 and 3 show a redward shift of low-n resonances and dissolution of high-n resonances. In addition, the background continuum is raised owing to redistribution of resonance strengths, which merge into one across high lying and overlapping thresholds.

4.2. Fe XVIII *: Scaling and delineation of resonances*

Next, we employ plasma broadened cross sections for Fe XVIII to highlight the scale, shape, scope, width and magnitude of AI resonances.

The scale of unbroadened AI features is evident upon a comparison on log and linear scales as in Fig. 4 (black curves), considered for two excited Fe XVIII levels. The top and bottom panels on left and right exhibit $Log\sigma_{PI}$(MB) and σ_{PI}(MB) respectively. Whereas the log-scale in top panels appropriately displays the full extent of AI resonances, it appears with equal weight for both positive values that rise up to 10^6 MB, and for negative values down to 10^{-6} MB that are not significant contributors, as shown in the bottom panels on a much smaller linear scale going from zero only up to 2.5 MB.

Attenuation of AI features due to plasma effects are shown in red and blue curves at two different T-D pairs; cross sections on the left are at a lower temperature and more than three times lower electron density than the ones on the right. Consequently, the AI features on the right in Fig. 4 are much more broadened that the ones on the left. Two other noticeable features are the closing of "opacity windows" in the unbroadened cross sections, and shift of AI resonances leading to temperature-density dependent redistribution of differential oscillator strengths and opacity with energy.

4.3. Conservation of differential oscillator strength

It is important to ensure the numerical accuracy of AI plasma broadening in temperature-density-energy space. Theoretically and computationally, that implies an investigation of integrated differential oscillator strengths proportional to σ_{PI} for all levels of a given ion for the three forms computed: (i) unbroadened (black curves), (ii) with all plasma broadening effects included as in Eq. (6) (red curves), and (iii) as in (ii) but with Stark ionization cut-off that leads to sharp step-wise structures below each

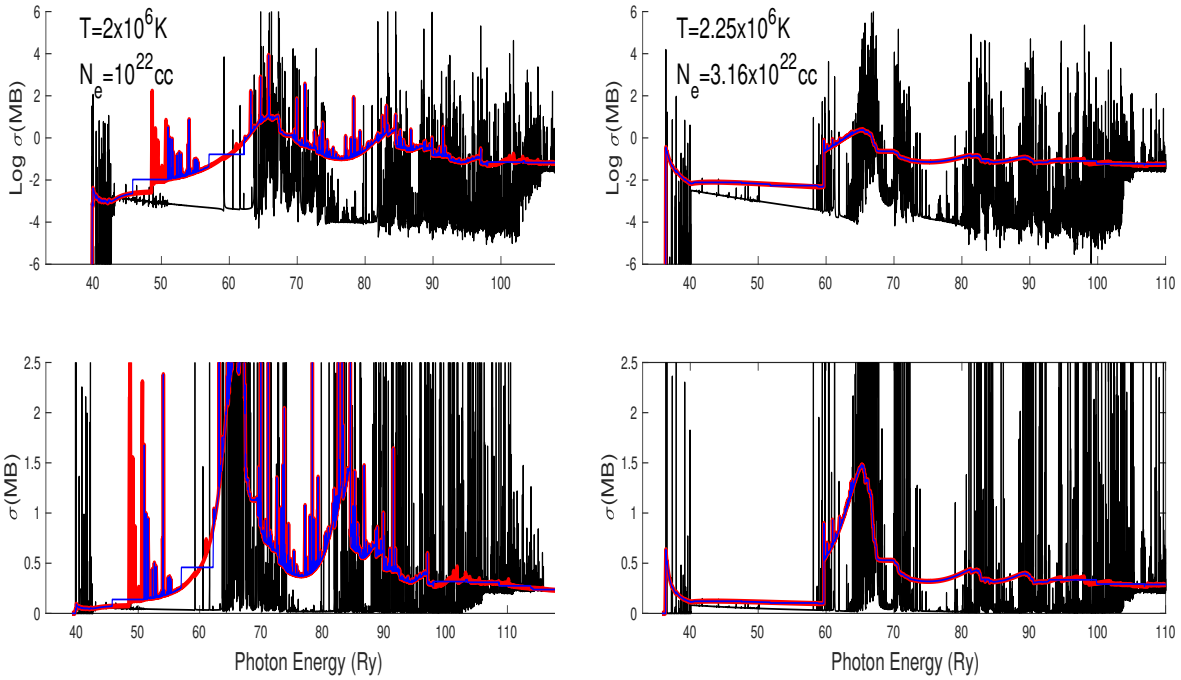

Figure 4. Plasma broadened photoionization cross sections on Log and linear scales, σ_{PI}(MB) (top panels) and $Log\sigma_{PI}$(MB) (bottom panels) for $\hbar\omega$ + Fe xviii $\rightarrow$ e + Fe xix of the bound level $2s^2p^5\ ^2P^o_{1/2}$ (left, ionization energy 98.903 Ry), and level $2s^22p^4(^1D^e_2)3p\ ^2F^o_{5/2}$ (right, ionization energy 39.1204 Ry): black — unbroadened, red — broadened, blue — broadened with Stark ionization cut-off ν^*_s (Table 1). Rydberg series of AI resonance complexes with $\nu_i \leq 10$ belonging to 276 excited Fe XIX levels.

ionization threshold (blue curves). We had quoted these values for one level of Fe XVII above in Fig. 3.

In Fig. 5 we present σ_{PI} for the ground state of Fe XIX $2s^2p^4\ ^3P^3$ (ionization energy 104.956 Ry), as well as an excited state $2s2p^4(^2S)3s\ ^1S^e$ (ionization energy 24.186 Ry). For these two cross sections of Fe XIX we find integrated values over the entire energy range shown to be 21.74, 22.98 and 22.90 for the unbroadened, broadened, and broadened with Stark ionization cut-off, respectively for the ground state, and 12.48, 13.57 and 13.56 respectively for the excited state (units are in MB-Ry though only the relative values are indicators of accuracy). The numerical agreement between the three sets of values is well within ∼10% indicating conservation of oscillator strength, despite some uncertainty in integration over extensive narrow and broad resonance structures that vary by nearly 20 orders of magnitude in height for $\sigma_{PI}(2s2p^4(^2S)3s\ ^1S^e)$, and widely disparate width distribution among Rydberg vs. Seaton PEC resonances described in RMOP2.

Generally, the agreement between the three sets of calculations for each level of each ion at each temperature-density is also an accuracy check of the plasma broadening treatment presented. Since there are hundreds of levels or each ion considered, there is

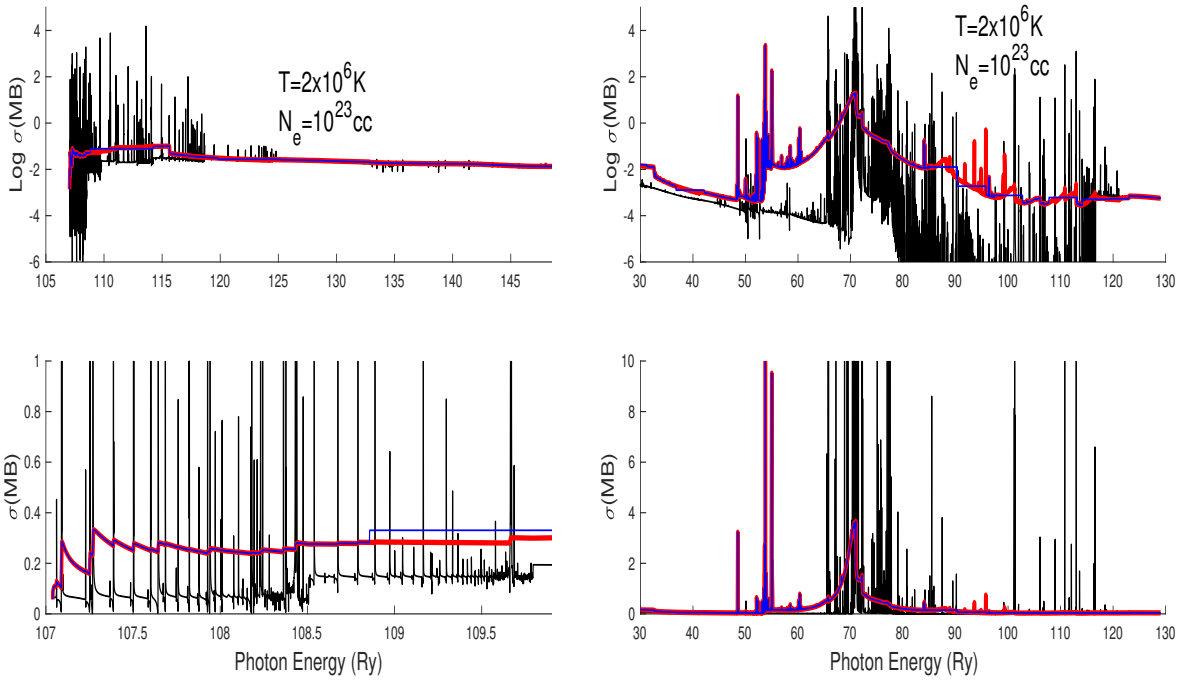

Figure 5. Plasma broadened photoionization cross sections on Log and linear scales, σ_{PI}(MB) (top panels) and $Log\sigma_{PI}$(MB) (bottom panels) for $\hbar\omega$ + Fe xix $\rightarrow$ e + Fe xx of the ground state $2s^2p^4\ ^3P^e$ (left), and $2s2p^4(^2S)3s\ ^1S^e$ (right): black — unbroadened, red — broadened, blue — broadened with Stark ionization cut-off ν_s^* (Table 2). AI resonances in the unbroadened σ_{PI} on the right range over 20 orders of magnitude.

more than 10% difference in integrated cross sections for highly excited levels at very high densities where the total AI width (Eq. 6) is very large. However, the highly excited levels are cut-off by the MHD-EOS and not considered in opacity calculations.

4.4. Plasma opacity parameters

Table 2 gives plasma parameters corresponding to Figs. 3. Their physical significance is demonstrated by a representative sample tabulated temperature T(K) and N_e . The maximum width γ_{10} corresponding to $\nu_i = 10$ in Eqs. (3,6) is set by the CC-BPRM calculations which delineate unbroadened AI resonance profiles up to $\nu \leq 10$, and employ an averaging procedure up to each threshold $10 < \nu < \infty$ using quantum defect (QED) theory (viz. [36, 12, 15] and references therein). $\gamma_c(10)$ and $\gamma_s(10)$ are the maximum collisional and Stark width components. The Doppler width γ_d is much smaller, 1.18×10^{-3} and 1.67×10^{-3} Ry at 10^6K and 2×10^6K respectively, validating its inclusion in Eq. (6) in HED plasma sources but possibly not when γ_d is comparable to γ_c or γ_s. The ν_s^* and ν_D are effective quantum numbers corresponding to Stark ionization cut-off and the Debye radius respectively. We obtain $\nu_D = \left[\frac{2}{5}\pi z^2\lambda_D^2\right]^{1/4}$, where the Debye length $\lambda_D = (kT/8\pi N_e)^{1/2}$. It is seen in Table 2 that $\nu_D > \nu_s^*$ at the T, N_e considered, justifying neglect of plasma screening effects herein, but which may need to

Table 2. Plasma parameters along isotherms in Fig. 2 and 3; ν_D corresponds to Debye radius; R is the ratio of Fe XVII Rosseland Mean Opacity with and without broadening [39]; γ_{10} is the maximum AI resonance width at $\nu = 10$.

T(K)	$N_e(cc)$	$\gamma_{10}(Ry)$ $\nu = 10$	$\gamma_c(10)$	$\gamma_s(10)$	ν_s^*	ν_D	R
2×10^6	10^{21}	3.42(-1)	8.55(-2)	2.57(-1)	10.4	28.1	1.35
2×10^6	10^{22}	2.05(0)	8.55(-1)	1.19(0)	7.7	15.8	1.43
2×10^6	10^{23}	1.41(1)	8.55(0)	5.53(0)	5.6	8.9	1.55
2×10^6	10^{24}	1.11(2)	8.55(1)	2.57(1)	4.1	5.0	1.58
10^6	$3.1 \times 10^{21.5}$	8.17(-1)	2.71(-1)	5.46(-1)	9.0	17.8	1.47
10^6	$3.1 \times 10^{22.5}$	5.25(0)	2.71(0)	2.53(0)	6.6	10.0	1.13
10^6	$3.1 \times 10^{23.5}$	3.89(0)	2.71(1)	1.18(0)	4.8	5.6	1.06

be accounted for at even higher densities.

The aggregate effect of AI broadening for large-scale applications is demonstrated in Table 2 by the ratio R of the Rosseland Mean Opacity (defined and discussed in RMOP1 Eqs. 1-4), at different temperatures and densities, using broadened/unbroadened cross sections for 454 Fe XVII levels with AI resonances (other higher bound levels have negligible resonances) [39, 35]. For any atom or ion R is highly dependent on T and N_e ; for Fe XVII R yields up to 58% enhancement due to plasma broadening with increasing N_e along the 2×10^6K isotherm, but decreasing to 6% along the 10^6K isotherm. Approximately 70,000 free-free transitions among +ve energy levels are included in the calculation of R, but their contribution has no significant broadening effect since they entail very high-lying levels with negligible level populations. However, different plasma environments with intense radiation fields, or a different equation-of-state than [31] employed here, may lead to more discernible effect due to free-free transitions. AI broadening in a plasma environment affects each level cross section differently, and hence its contribution to opacities or rate equations for atomic processes in general. A critical (T,N_e) range can therefore be numerically ascertained where redistribution and shifts of atomic resonance strengths would be significant and cross sections should be modified. Overall opacity enhancement depends not only on AI resonance broadening at a given temperature-density but also on the equation-of-state [40].

4.5. Relative broadening effects

Following Table 1 we can examine the individual effects of including different broadening mechanisms separately in the combined total (Eq. 6). Fig. 6 shows the cross sections including the three dominant mechanisms. Referring to Fig. 3 for photoionization of Fe XVIII and Table 1, the contributions are shown due to Eq. (21) for collisional (cyan), Eq. (25) for thermal (magenta), and Eq. (24) for Stark (green) effects respectively. Results are given in Fig. 6 for $T = 2 \times 10^6$K at two electron densities $10^{21}/cc$ (left) and

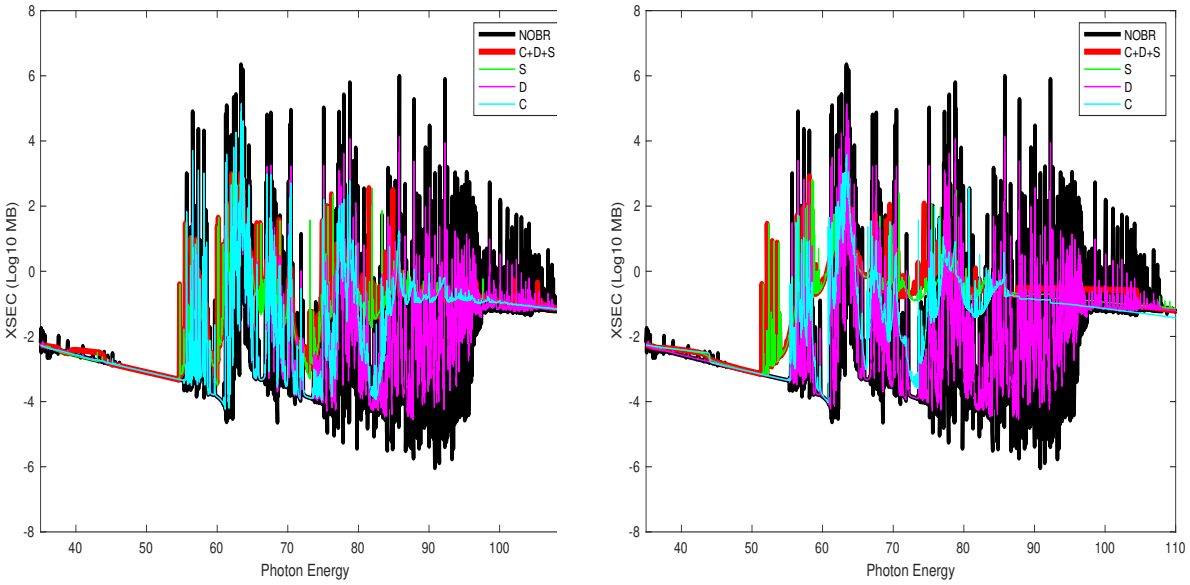

Figure 6. Effect of including individual broadening mechanisms on photoionization cross sections in Fig. 3 for isotherm $T = 2 \times 10^6$ K, $N_e = 10^{22}/cc$ (Left) and $N_e = 10^{23}/cc$ (Right): unbroadened (black), total broadened (red), C—Collisional (cyan), D—Doppler Thermal (magenta), S—Stark (green).

$10^{23}/cc$ (right). From Table 1 we see the relative widths due to collisional and Stark broadening; thermal (Doppler) broadening is much smaller and manifests itself for only for very narrow resonances and high-lying thresholds. At the lower density (left) much of the unbroadened resonance structures (black) are discernible although significantly dissolved, and collisional width is less than Stark width which is larger (Table 1) and closer to the total broadened cross sections (red). At the higher density (right) the effects of collisional and Stark are reversed; the former is more prominent though quite comparable to the latter. More detailed studies on a number of cross sections for different ions would be needed to ascertain precisely the broadening effects in each case. However, from the limited results presented herein a conservative estimate is that the lower density limit for broadening mechanisms to manifest themselves is $N_e > 10^{20}/cc$. Table 1 also indicates probable high density limit at $N_e > 10^{24}/cc$ based on two reasons: (i) the total combined AI broadening widths become very large and comparable to the entire energy range of the resonance structures included in computations of cross sections, and (ii) the Debye lengths are comparable to or shorter than bound electronic orbital radii, and atomic configurations are no longer a viable description which would require dense plasma effects to be considered non-perturbatively.

5. Conclusion

The main conclusions are: (I) The method described herein is generally applicable to AI resonances in atomic processes in HED plasmas. (II) The cross sections become

energy-temperature-density dependent in a critical range leading to broadening, shifting, and dissolving into continua. (III) Among the approximations necessary to generalize the formalism is the assumption that thermal Doppler widths are small compared to collisional and Stark widths as herein, but given the intrinsic asymmetries of AI resonances it may not lead to significant inaccuracies (although that needs to be verified in future works). (IV) The treatment of Stark broadening and ionization cut-off is *ad hoc*, albeit based on the equation-of-state formulation [31] and consistent with previous works [12]. (V) Since it is negligibly small, the free-free contribution is included post-facto in the computation of the ratio R in Table 2 and not in the cross sections and results shown in Figs. 2 and 3, but may be important in special HED environments with intense radiation and should then be incorporated in the main calculations of total AI width (Eq. 6). (VI) The predicted redward shift of AI resonances as the plasma density increases should be experimentally verifiable. (VII) Redistribution of AI resonance strengths should particularly manifest itself in rate coefficients for (e + ion) excitation and recombination in plasma models and simulations, and for photoabsorption in opacity calculations, using temperature-dependent Maxwellian, Planck, or other particle distribution functions. (VIII) The treatment of individual contributions to AI broadening may be improved, and the theoretical formulation outlined here is predicated on the assumption that external plasma effects are perturbations subsumed by and overlying the intrinsic autoionization effect. (IX) The computational formalism is designed to be amenable for practical applications and the computational algorithm and a general-purpose program AUTOBRO are optimized for large-scale computations of AI broadened cross sections for atomic processes in HED plasma and astrophysical models.

Data Availability statement

The unbroadened cross section data are available as reported in RMOP2. Broadened cross sections may be computed by contacting the author.

Acknowledgments

I would like to thank Sultana Nahar for atomic data for Fe ions and discussions.

References

[1] Griem H R 2005 *Principles of Plasma Spectroscopy*, Cambridge University Press
[2] Peach G 1981 *Advances in Physics* 30 367
[3] Konjevic N 1999 *Phys. Repts.* 316 339
[4] Djurovic S and Konjevic N 2009 *Plasma Sources Sci. Techol.* 18 030511
[5] Burke P G 2011 *R-Matrix Theory of Atomic Collisions* Springer
[6] Kelleher D E, Deipech J F and Weiner J 1985 *Phys. Rev. A* 32 2230
[7] Xiang W, Zeng J, Fu Y and Gao C 2012 *Journal of Modern Physics* 3 1670
[8] Cooper J W and Saloman E B 1982 *Phys. Rev. A* 26 1452

[9] Fano U 1961 *Phys. Rev. A* 124 1866
[10] Drake R P 2006 *High Energy Density Physics*, Springer
[11] Hubeny Ivan and Mihalas Dimitri 2015 *Theory of Stellar Atmospheres* Princeton University Press
[12] The Opacity Project Team, 1995 *The Opacity Project*, Institute of Physics Publishing, Vol 1
[13] Seaton M J, Yu Y, Mihalas D and Pradhan A K (SYMP) 1994 *Mon. Not. R. astr. Soc.* 266 805
[14] Hummer D G, Berrington K A, Eissner W, Pradhan A K, Saraph H E and Tully J A 1993 *Astron. Astrophys.* 279, 298
[15] Pradhan A K and Nahar S N 2011 *Atomic Astrophysics and Spectroscopy* Cambridge University Press
[16] Hubney I and Mihalas D 2014 *Theory of Stellar Atmospheres* Princeton University Press; Mihalas D 1978 *Stellar Atmospheres* Freeman
[17] Fano U 1961 *Physical Review* 124 1866
[18] Dimitrijevic M S and Konjevic N 1981 *Astron. Astrophys.* 102 93
[19] Dimitrijevic M S and Konjevic N 1987 *Astron. Astrophys.* 172 345
[20] Krief M, Feigel A and Gazit D 2016 *Astrophys. J.* 824 98
[21] Gigosos M A 2014 J. Phys. D 47 343001
[22] Yu Y and Seaton M J *J. Phys. B* 20 6409
[23] Palmeri P, Quinet P, Mendoza C, Bautista M, Withoeft M C and Kallman T R 2016 *Astron. Astrophys.* 589 A137
[24] Gatuzz E, Gorczyca T W, Hasoglu M F, Schulz N S, Corrales L and Mendoza C 2020 *Mon. Not. R. astr. Soc.* 498 L20
[25] Several formulations were investigated and employed to implement a Voigt profile used in line broadening work (viz. [26, 27, 28] and later works). They were found to be numerically unstable owing to required limits on the relative widths of AI broadening mechanisms considered herein, that rendered the Voigt kernel mathematically ill-conditioned and computationally impractical. For example, the parameter related to the ratio collisional-to-Doppler widths $\gamma_c/\gamma/_d$, that is usually evaluated and specified for line broadening and assigned numerical limiting values in integration, is not practical since $\gamma_c >> \gamma_d$ at temperatures and densities of interest in HED plasmas.
[26] Hummer D 1965 *Mon. Not. R. astr. Soc.* 70 1
[27] Hui A K, Armstrong B H and Wray A A 1978 *J. Quant. Spectrosc. Radiat. Transfer* 19 509
[28] Huang X and Yung Y L 2004 *Amer. Meteor. Soc.* 61 1630 (and references therein)
[29] Seaton M J 1990 *J. Phys. B* 23 3255
[30] The OP work [12] consists of treatment of line broadening implemented by M J Seaton in four papers in the series *Atomic Data for Opacity Calculations* (ADOC) — ADOC-I, ADOC-V, ADOC-VIII and ADOC XIII [29].
[31] Mihalas D, Hummer D G and Däppen W 1988 *Astrophys. J.* 331, 815
[32] Inglis D R and Teller E 1939 *Astrophys. J.* 90 439
[33] Seaton M J 2000 *J. Phys. B* 33 2677
[34] Nahar S N, Pradhan A K, Chen G.-X and Eissner W 2011 *Phys. Rev. A* , 83, 053417
[35] Nahar S N and Pradhan A K 2016 *Phys. Rev. Lett.* 116 235003; Ibid. *Phys. Rev. Lett.* , 117, 249502
[36] The QD regions $10 < \nu_i < \infty$ are generally small and overlapping for closely spaced excited core levels, as herein.
[37] Eissner W, Jones M and Nussbaumer H 1974 *Comput. Phys. Commun.* 8 270
[38] Xiang W, Zeng J, Fu Y and Gao C 2012 *J. Mod. Phys., 3, 1670*
[39] We eschew a discussion of opacities *per se*, as they also depend on accuracy and completeness of atomic data, equation-of-state of the plasma source and other quantities, and focus on AI resonance broadening in atomic processes.
[40] Pradhan A K 2024 *Mon. Not. R. astr. Soc.* 527 L179
[41] Cowan R D 1981 *The Theory of Atomic Structure and Spectra* University of California Press Berkeley CA USA